Linear patterning of magnetically labeled *Dictyostelium* cells to display confined development

Linear patterning of magnetically labeled *Dictyostelium* cells to display confined development

Guillaume Frasca, Franck Raynaud, Jean-Claude Bacri, Florence Gazeau and Claire Wilhelm

Laboratoire Matière et Systèmes Complexes (MSC), UMR 7057 CNRS et Université Paris-Diderot, Paris, France

E-mail: claire.wilhelm@univ-paris-diderot.fr

Abstract

In severe nutriment conditions, the social amoeba *Dictyostelium discoideum* enters a particular life cycle where it forms multicellular patterns to achieve aggregation. Extensively observed from an initial dispersed state, its developmental program can usefully be studied from a confined population to implement theoretical developments regarding biological self-organization. The challenge is then to form a cell assembly of well-defined geometrical dimensions without hindering cell behavior. To achieve this goal, we imposed transient constraints by applying temporary external magnetic gradients to trap magnetically labeled cells. Deposits of various numbers of cells were geometrically characterized for different magnetic exposure conditions. We demonstrated that the cell deposit was organized as a three-dimensional (3D) structure by both stacking layers of cells and extending these layers in the substrate plane. This structure evolves during the aggregation phase, forming periodic aggregative centers along the linear initial pattern.

(Some figures in this article are in colour only in the electronic version)

1. Introduction

The multicellular organism *Dictyostelium discoideum* is a powerful, accessible and simple model system widely used for studying a variety of basic development processes, including intercellular communication [1], chemotaxis, cell motility and spatial patterning [2].

In normal food conditions, *Dictyostelium* consists of individual free living cells. After being nutrient-deprived, the once single cells enter an aggregation phase where they migrate, forming stream patterns, to gather to a finite number of aggregation centers. They then form a mound which evolves into a motile slug and finally a fruiting body.

Most of the current knowledge regarding *Dictyostelium* pattern formation [3] has been obtained through the *in vitro* analysis of spontaneous aggregation of *Dictyostelium* cells when first homogeneously spread on conventional Petri dishes. Initiation of the morphogenetic program has not yet been explored from an initial dense and confined assembly of individual cells, which could more likely mimic *in vivo* biological conditions. Indeed, when starvation induces the aggregation process, cells are not likely to be uniformly dispersed on a natural substrate, but more probably gathered in some sort of pre-existing patterns due to the *in vivo* substrate specificities. Here we aimed at localizing *in vitro Dictyostelium* cells in a controlled 3D linear pattern, during the pre-aggregating stage, to observe morphogenesis from an initial confined state.

Two-dimensional (2D) micro-patterned substrates are usually well fitted to create such multicellular organization [4, 5]. However, as the micro-structures are based on chemical modification of the substrate, it would frustrate the genuine self-organization process. Besides, it is unlikely that we could obtain a well-defined 3D cell structure by imposing constraints solely on the planar substrate. Here we magnetically labeled *Dictyostelium* cells with magnetic nanoparticles and used an external magnetic force to achieve cell patterning.
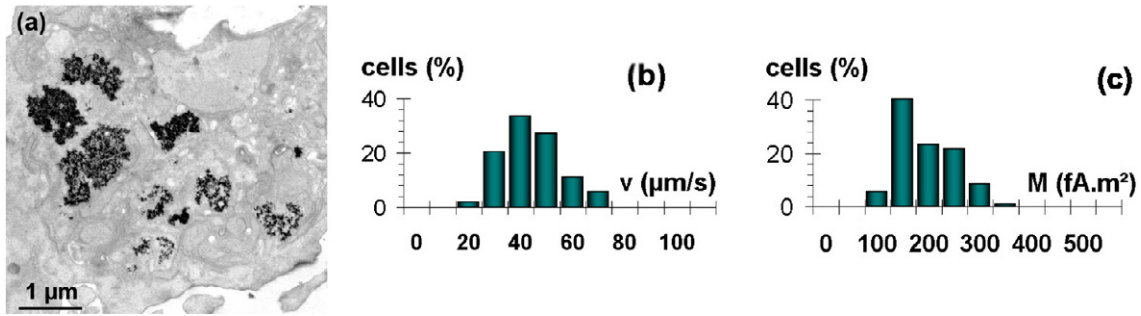
Figure 1. (a) Electron micrograph of a *Dictyostelium* cell incubated with magnetic maghemite nanoparticles (1 h, [Fe] = 2 mM). The particles are electron dense and appear as black points on the images. Particles are packed within micron-sized intracellular vesicles, named endosomes. (b) Distribution of the cell velocity v for 200 measured cells. (c) Equivalent distribution of the magnetic moment M calculated from the forces balance: $M\,\mathrm{grad}\,B = 6\pi\eta Rv$, with R the cell radius. Distributions slightly differ because the distribution of cell radius among the population was also taken into account.

The magnetic label was high enough to control *Dictyostelium* migration using a thin magnetic tip [6]. Here we show we could magnetically guide cell adhesion using external magnets (first demonstrated by Ito *et al* for fibroblasts and endothelial cells in [7]). The magnetic field was created using magnetized thin steel plates placed perpendicular under the dish onto which cells adhere. Magnetic field gradients were carefully calibrated using well-calibrated fluorescent magnetic beads. We then fully characterized the formation of magnetic cells lines, varying both the number of cells per line and the time of magnetic exposure to form cohesive 3D structures. Finally, we observed the formation of intriguing patterns when starved confined *Dictyostelium* cells enter the aggregation phase.

2. Materials and methods

2.1. Cell culture and magnetic labeling

$A \times 2$ *Dictyostelium* cells were grown at 21 °C in shaken glass flasks (100 rpm) in axenic medium (HL5 medium supplied by Formedium) supplemented with 50 units ml^{-1} penicillin. At a cell concentration of 10^7 cell ml^{-1}, iron oxide maghemite magnetic nanoparticles were added to the medium at an iron concentration of 2 mM for 1 h. Intracellular localization of magnetic particles was assessed by electron microscopy (Zeiss EM902 microscope, 70 nm sections of Epon embedded cells). For line formation and development, cells are dispersed, after magnetic labeling, in phosphate buffer (KK2: KH$_2$PO$_4$ 16.5 mM, K$_2$HPO$_4$ 3.8 mM, pH = 6.3).

2.2. Quantification of the magnetic load per cell (magnetophoresis)

The migration of magnetically labeled cells towards a permanent magnet was followed by video-microscopy. In the observation window, the mean magnetic field equals 0.145 T with a uniform magnetic field gradient (grad B = 17 mT mm^{-1}). The cells therefore migrate at constant velocities and we determine the magnetic moment M carried by each cell by simply balancing the magnetic force ($M\,\mathrm{grad}\,B$) with the viscous one ($6\pi\eta Rv$, R and v being respectively the

cell radius and velocity, η being the water viscosity equal to 10^{-3} Pa s) [8].

2.3. Formation of linear 3D deposits of magnetic cells

A 10 cm long, 1 cm thick and 500 μm wide plate made of soft iron was magnetized with a rectangular magnet (1 cm × 4 mm × 10 cm) developing a magnetic field of (0.14 ± 0.02) T at about 100 μm from the surface. The magnetic field gradient generated by the plate was carefully calibrated experimentally using fluorescent magnetic beads of 4.6 μm diameter (magnetic moment: $(2 \pm 0.4) \times 10^{-13}$ A m^2). For cell linear patterning, 4 μl of a dense suspension of magnetic cells (from 4×10^4 to 6×10^6 cells) was then carefully deposited along the magnetic band.

3. Results and discussion

3.1. Efficient magnetic labeling of Dictyostelium cells

Magnetic nanoparticles enter the cells through the endocytotic pathway and concentrate inside pre-existing intracellular vesicles named endosomes (figure 1(a)), conferring to the whole cell high magnetic properties. The magnetic content distribution over the cell population was quantified by measuring the velocity of 200 migrating cells in the magnetophoresis set-up. A typical distribution of the velocities is presented in figure 1(b). The magnetic moment of one cell is distributed around $M = 1.7 \times 10^{-13}$ A m^2 when submitted to a magnetic field of 0.145 T (figure 1(c)), with deviation of 35% reflecting the variability of endocytic capacities among the cell population.

3.2. High magnetic field gradient developed by a laminated soft iron band

To calibrate the magnetic field gradient created by the soft iron magnetized band (figure 2(a)), the movement of fluorescent magnetic beads in 98% v/v glycerol ($\eta_{\mathrm{glycerol}} = 0.94$ Pa s at room temperature) was followed in the yz plane paved with squares of 200 μm × 200 μm. We measured the velocities of around 25 beads passing through each square. Assuming
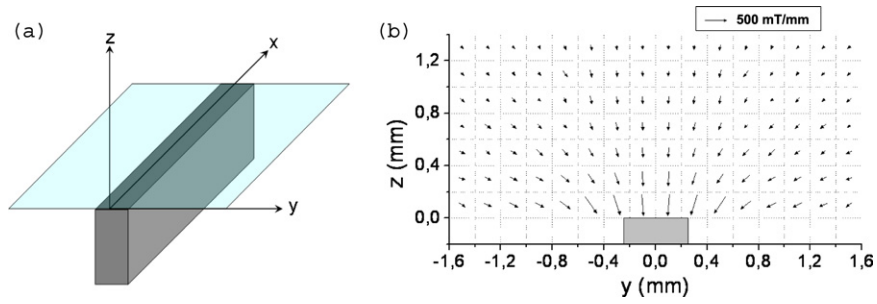
Figure 2. (a) Scheme of the magnetic device; (b) magnetic field gradients in the yz plane.
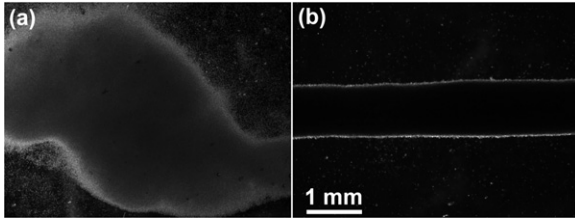

Figure 3. Phase contrast microscopy of the linear pattern:
(a) 1.4×10^6 magnetic cells concentrated in 4 μl, deposited with a micropipette along the non-magnetized band line; (b) same deposit along the magnetized band.

surface is positioned 100 μm away from the band line (figure 2(b)).

The band is magnetized by a permanent magnet. Figure 3 shows the different patterns observed for the deposited cell suspension when the band is magnetized (b) or not (a). Clearly, no linear pattern is observed without any driving magnetic force, even if the cells are deposited at the vicinity of the band onto the substrate. By contrast, if concentrated cells are properly deposited along the magnetized band line, we observe a clean linear pattern, with almost no adhered cells outside the line.

inertia was negligible, the magnetic field gradient was deduced from the balance of the magnetic and viscous forces.

Figure 2(b) shows the resulting magnetic field gradient values, attaining $(4.5 \pm 1.2) \times 10^2$ mT mm^{-1} in the band direction (corresponding to the closest squares from 0 to 200 μm from the band line). In the z direction, the magnetic force experienced by a magnetic cell bearing a mean moment $M = 1.7 \times 10^{-13}$ A m^2 attains 80 pN at 100 μm from the line, equivalent to a cell velocity of 1.4 μm s^{-1}.

3.3. Magnetic linear cell patterning

A 16 mm diameter cylindrical chamber sealed with a 100 μm thick glass slide, filled with KK2 phosphate buffer, was deposited on the soft iron band slice, so that the cell adhering

3.4. Characterization of the linear pattern

From 4×10^4 to 6×10^6 cells, concentrated into 4 μl, were deposited in line along the magnetic band. The entire line was observed both by a high zoom lens camera (figure 4—top of each part) and by video-microscopy, using a 1.6× objective (figure 4—bottom of each part). The magnetic force applied on the deposited cells imposes a 3D confinement, the efficiency of which was fully characterized.

For a large number of deposits, for both a 10 min- and a 2 h-long adhesion on the magnetized band, the whole line area A was measured and both width and length were estimated from the dimensions of the bounding rectangle (figure 4(a)). To mask a slight dispersion of line lengths ($L = (11.54 \pm 1.34)$ mm), mostly due to experimental deviations during the deposit, the measured area A was renormalized to the area of the
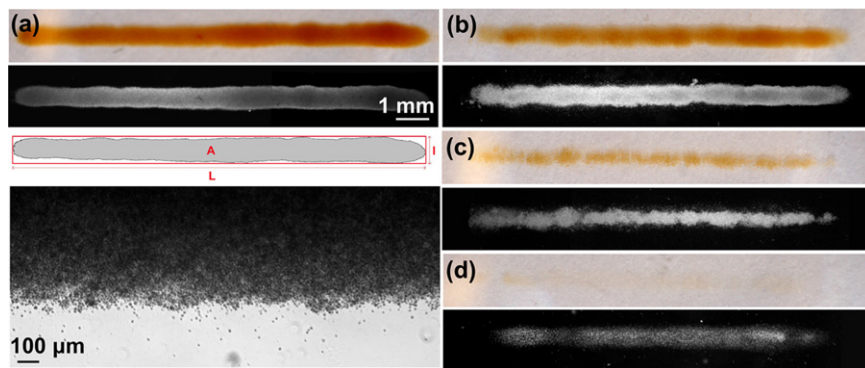

Figure 4. (a) $(1.2 \pm 0.1) \times 10^6$ *Dictyostelium* cells deposit on the magnetized soft iron band. Top: images of a high zoom camera and 1.6× phase contrast microscopy; middle: characteristic geometrical parameters deduced from image analysis (area A, length L and width l); bottom: 4× transmission microscopy image of the line to observe individual cells at the border; (b) $(0.6 \pm 0.05) \times 10^6$ cells; (c) $(1.5 \pm 0.1) \times 10^5$ cells; (d) $(0.4 \pm 0.02) \times 10^5$ cells.
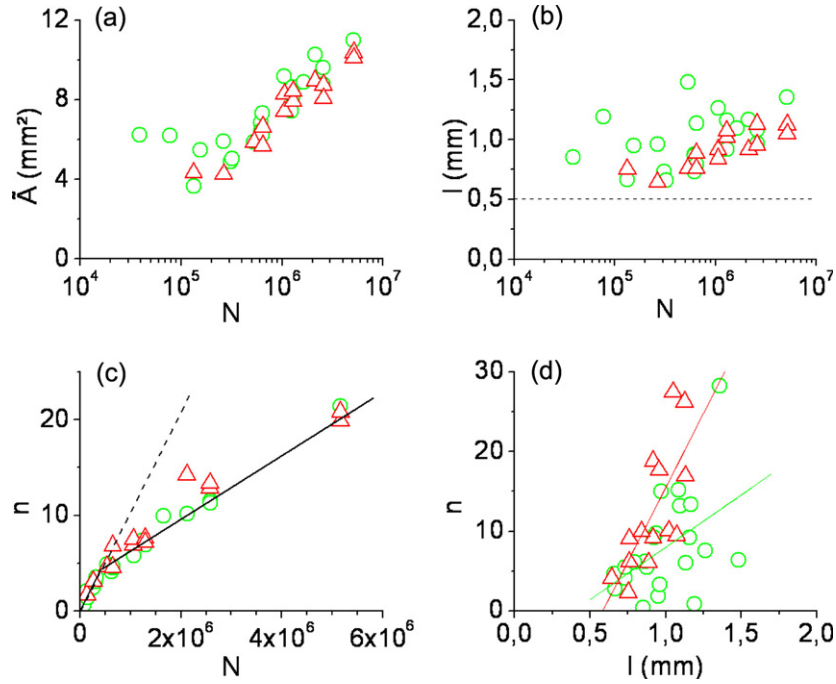
Figure 5. Geometrical characteristics of the linear pattern for different numbers of deposited cells N, for both 10 min- (○) and 2 h-long (△) magnetic adhesion: (a) renormalized total adhesion area $\tilde{A}$; (b) line width l; (c) number of layers n; (d) number of layers n as a function of l.

equivalent line of mean length $\langle L \rangle$, described as $\tilde{A} = A \cdot \langle L \rangle / L$ in figure 5(a) as a function of the deposited number of cells N. This parameter describes the maximal extension of the cells around the magnetic band.

For the lowest cells number, the linear deposit is not homogeneous (figure 4(c)), presenting important density and extension variations along the line axis x. The line width l can then be interpreted as the maximal width of the deposit, and reflects the extent of the magnetic driving force in the y direction. Figure 5(b) shows this maximum width as a function of the number of cells deposited onto the dish, to be compared to the magnetic band width $l_{band} = 0.5$ mm.

The normalized line area $\tilde{A}$, which is nearly constant for the smallest numbers of cells, increases for N above a critical value $N_c \approx 3 \times 10^5$ cells. By contrast, no clear behavior is seen for the dependence of the line width l with the number of cells deposited. The mean widths for both magnetic field exposure conditions are very similar: $l(10\ \text{min}) = (0.99 \pm 0.22)$ mm and $l(2\ \text{h}) = (0.92 \pm 0.15)$ mm. It shows that lateral maximal extension of the deposit tends to be independent of the deposit concentration and the magnetic exposure duration and controlled solely by the magnetic band width. The deposit area increase with the number of cells is mostly due to a higher efficiency in the magnetized band coverage by the cells dispersed in its vicinity. This 2D phenomenon is coupled to a 3D enlargement of the cell stack in the z direction when N increases.

To estimate the rough number of layers of cells stacked in the linear deposit, we approximated the cells as hard spherical objects. Cell diameters measured for 1000 cells were distributed around 7.6 μm ($d = 7.6 \pm 1.2\ \mu$m). One highly compacted layer with N' spheres of diameter d fills an area of
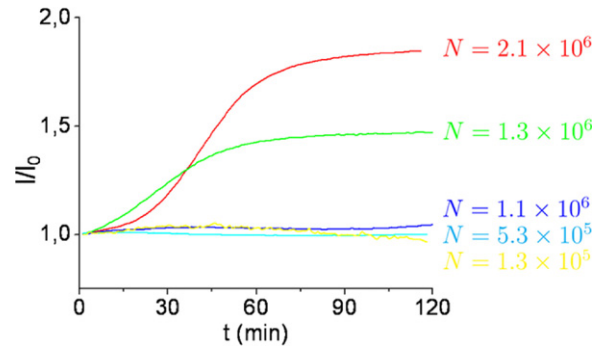

Figure 6. Spreading of a linear deposit after 10 min for five different numbers of cells. For dense deposits, the lateral extension increases within 1 h to reach a stable organization, whereas small deposits stay cohesive with time.

$\frac{2\pi}{1+\sqrt{3}/2} N' d^2 = 0.84 N' d^2$. Consequently, an estimate of the number of layers for an N cells deposit is $n = 0.84 N d^2 / A$. This number of layers n is represented in figure 5(c) as a function of the number of cells in the line. Two linear regimes are observed, defining a threshold value $N_c = 3 \times 10^5$ cells. For $N < N_c$, A is constant and n increases rapidly from 1 to 4 piled layers: the line assembly is mostly developed in the z direction by piling up more and more cell layers. For $N > N_c$, A increases and n increases more slowly than before with the number of cells. If the cells keep piling up layers in a 3D stack, the 2D extension of the line deposit now increases more dramatically with N. Finally, the number of layers n was represented as a function of the line width l (figure 5(d)), pointing out different behaviors depending on the magnetic exposure conditions. For a 10 min- and 2 h-long
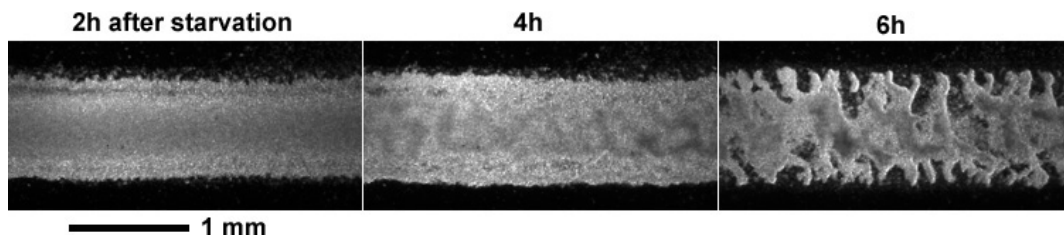
Figure 7. Dynamics of a 10^6 cell linear deposit after a 10 min long magnetic exposure, in starvation conditions (phase contrast microscopy).

magnetic exposition, a lateral extension increase corresponds to a stacking one. But the slope is steeper for a 2 h-long adhesion: the longer the magnetic exposure stands, the more efficient the lateral confinement and the layer stacking are. In these experimental conditions, one then can obtain more easily a thinner (decreased width l) and/or thicker (increased number of layers n) linear deposit and then a more circumscribed pattern.

3.5. Spreading of the cell 3D linear deposit

To further characterize the magnetically induced confinement of labeled cells in linear structures, we observed by video-microscopy the temporal evolution of the cell lines without magnetic force, after a 10 min long exposure to the patterning magnetized band. The 'magnetic-free' line extension is measured by the ratio $l(t)/l_0$ of the line width by the initial width after a 10 min long formation on the magnetic band, as shown in figure 6 for five different numbers of deposited cells. 'Small' lines containing less than about 1.2 million cells (for an average line length of about 12 mm) stay cohesive for more than 2 h without magnetic force. By contrast, lines containing more than 1.2 million cells start spreading about 15 min after the end of magnetic exposure. The higher the number of cells, the more important the spreading is.

3.6. Early development pattern for cells confined in line

Upon starvation, in the phosphate buffer, the cells of the 3D linear stack enter the developmental stage, mediated by waves of the cell-secreted chemoattractant cAMP (cyclic adenosine monophosphate). We previously demonstrated that, 10 h after the beginning of starvation, magnetically labeled *Dictyostelium* cells could be controlled by a thin magnetic tip [6]. Here, the aggregation center is unique, with a linear pattern. Lines of one million cells are observed through video-microscopy for 18 h after the beginning of starvation. Figure 7 shows the developmental stages of such a line. Most mathematical models for spatial patterning in *Dictyostelium* are based on continuum models of the cAMP concentration and cell density

fields [9]. Here we suggest that the observed patterns are due to the confined boundary conditions of the 3D multicellular aggregate. We plan to model this system as a set of reaction-diffusion equations for the concentration fields of cAMP coupled with cell velocity fields according to the Navier–Stokes equation.

4. Conclusion

We developed here an original procedure to form a cell aggregate with well-defined geometrical dimensions. *Dictyostelium discoideum* cells are magnetically labeled by the internalization of maghemite nanoparticles and then trapped in the vicinity of a magnetized device. The applied magnetic force confines millions of cells deposited onto the substrate to form a linear pattern. This cell assembly was fully characterized and we demonstrated the cell organization results of the 3D stacking of layers of cells and the lateral extension in the substrate plane. We showed that the pattern cohesion depends on both the duration of the magnetic exposure and the number of cells. This linear stacking appears to be a valuable assay to further explore the developmental program of *Dictyostelium* from an initial confined state where cell density is close to the aggregation phase situation.

References

[1] Maeda Y 2005 *Int. Rev. Cytol.* **244** 287–332
[2] Turing A M 1952 *Phil. Trans. R. Soc.* B **237** 37–72
[3] Dormann D, Vasiev B and Weijer C J 1998 *Biophys. Chem.* **72** 21–35
[4] Zhang S, Yan L, Altman M, Lssle M, Nugent H, Frankel F, Lauffenburger D A, Whitesides G M and Rich A 1999 *Biomaterials* **20** 1213–20
[5] Nahmias Y, Arneja A, Tower T T, Renn M J and Odde D J 2005 *Tissue Eng.* **11** 701–8
[6] Wilhelm C, Rivière C and Biais N 2007 *Phys. Rev.* E **75** 041906
[7] Ino K, Ito A and Honda H 2007 *Biotechnol. Bioeng.* **97** 1309–17
[8] Wilhelm C, Gazeau F and Bacri J C 2002 *Eur. Biophys. J.* **31** 118–25
[9] Kessler D A and Levine H 1993 *Phys. Rev.* E **48** 4801–4